Engineering Structures 167 (2018) 420–430

Contents lists available at ScienceDirect

Engineering Structures

journal homepage: www.elsevier.com/locate/engstruct

Experimental tests on multiple-slit devices for precast concrete panels

Bruno Dal Lago*, Fabio Biondini, Giandomenico Toniolo

Department of Civil and Environmental Engineering, Politecnico di Milano, Piazza Leonardo da Vinci 32, 20133 Milan, Italy

ARTICLE INFO

Keywords:
Precast structures
Concrete panels
Energy dissipation
Plasticity
Friction
Experimental testing

ABSTRACT

Multiple Slit Devices (MSDs) are plasticity-based dissipative connectors consisting of steel plates provided with slits which lead to a set of elementary beams. In this way, the shear-type behavior of the plate is turned into the flexural-type behavior of the elementary beams, which ensures better energy dissipation. The proposed MSDs are bolted to support steel profiles inserted into appropriate recesses in between precast concrete panels to improve the seismic performance of the earthquake-resisting system. The paper presents the results of monotonic and cyclic experimental tests performed on both connectors and structural sub-assemblies consisting of two full-scale precast concrete panels connected by a MSD. Steel plates with slits of various shape and size are considered. An improved version of the connector capable to dissipate energy through both plasticity and friction and to provide enhanced displacement capacity is also proposed and tested.

1. Introduction

The seismic performance of structural systems can be significantly improved by means of dissipative systems of connections. Multiple Slit Devices (MSDs) are connectors made of steel plates provided with slits which lead to a set of elementary beams dissipating energy based on steel plasticity. The slits can be achieved using different technologies, including laser cutting. When subjected to lateral load, the shear-type behavior of the plate is turned into the flexural-type behavior of the elementary beams, which ensures better energy dissipation based on steel plasticity and higher displacement capacity. The yielding and ultimate strengths of the device depend on both the shape and size of the elementary beams.

This type of device has been developed mainly for use in steel structures and can be considered as an evolution of the Added Damping And Stiffness (ADAS) devices [1–6], where slender butterfly-shaped steel beams are linked together and dissipate energy through plasticity. Several types of plate dissipative devices have been tested by Chan et al., including buckling restrained plates [7], multiple slits with constant depth elementary beams [8], and perforated plates [9]. Oh et al. carried out experimental testing on full scale beam-to-column steel joints enhanced with MSDs [10]. Structural optimization procedures have been applied by Ghabraie et al. to achieve an optimized MSD with hourglass-shaped elementary beams that was also experimentally tested [11]. Recently, Briones and de la Llera developed a metallic dissipative connector based on hourglass-shaped copper elements [12]. Ma et al. developed design procedures and experimental tests on MSDs with different beam depth profiles, including constant and butterfly-shaped profiles [13]. Analytical design tools have been proposed also by Karavasilis et al. [14]. Lee et al. performed experimental and numerical investigations on MSDs where plasticity and friction are exploited for energy dissipation [15].

Several types of dissipative devices can be used for precast structures [16–22]. It has been shown that different types of dissipative systems of connections applied to the cladding wall panels allow to limit the base shear and significantly reduce the drift and consequent damage of precast structures under seismic actions [23–26]. The MSDs investigated in this paper have been specifically designed for use in precast concrete structures as panel-to-panel dissipative connections [27,28].

In the proposed MSDs, the steel plates are bolted to support steel profiles that are inserted into recesses at the interface between adjacent panels, as shown in Fig. 1a. The functioning scheme of the MSD under imposed relative panel-to-panel displacement is shown in Fig. 1b. The MSD is made by mounting two steel plates on support profiles of various shapes. Fig. 2 shows the assembled MSD supported by T-shaped (Fig. 2a), UPN (Fig. 2b), and angle steel profiles (Fig. 2c). For installation, T-shaped and UPN profiles need access from both sides. In addition, UPN profiles need at top and bottom sides larger free room for tightening the internal bolts that connect the profiles to the sockets embedded in the concrete panel. Asymmetric angle profiles involve eccentric forces and torsional actions but need small recesses and allows for installation from one side only, which might be mandatory for application to sandwich concrete panels.

* Corresponding author.
E-mail address: brunoalberto.dallago@polimi.it (B. Dal Lago).

https://doi.org/10.1016/j.engstruct.2018.04.035
Received 12 September 2017; Received in revised form 13 March 2018; Accepted 9 April 2018

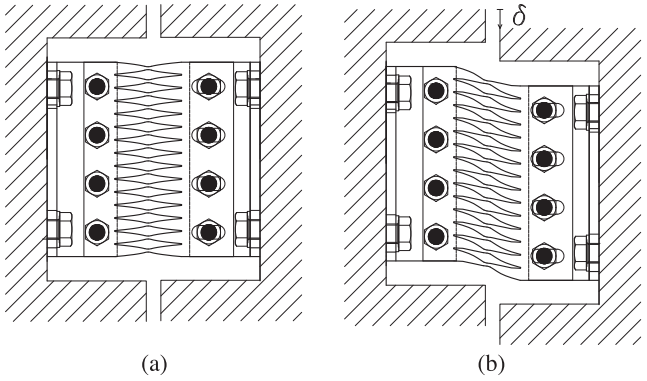

Fig. 1. MSD for precast panels: (a) assembled connection; (b) deformed configuration.

An experimental campaign has been performed at Politecnico di Milano within the framework of the SAFECLADDING research project funded by the European Commission to provide guidelines for a proper seismic design of precast structures with cladding panels and to propose innovative systems of connections [29]. The mechanical characterization of MSDs provided with steel plates with slits of various shapes and sizes have been performed as part of this research project based on monotonic and cyclic experimental tests carried out on both single connectors and structural sub-assemblies consisting of two full-scale concrete panels. An improved version of the connector capable to dissipate energy through both plasticity and friction and to provide a larger displacement capacity has been also developed and tested. The results of the experimental tests are presented and discussed, and design criteria for the MSD device are finally proposed.

2. Experimental tests on connectors

Local tests have been carried out on MSDs under imposed lateral displacements to characterize their mechanical behavior and their stability under cyclic loading at both small and large amplitude displacements.

2.1. Test specimens

The MSDs conceived and tested are shown in Fig. 3. The specimens have been designed with a span to depth ratio of the single elementary beam not larger than four, in order to avoid lateral (flexural-torsional) buckling. The thickness of the plates has been considered not larger than 5 mm, in order to be easily wrought by standard laser cutters. The need of maximizing the area of steel that had to yield led to devices with no more than two lines of slender beams with constant depth profile (specimens type I and type II). Devices with elementary beams having hourglass profile with uniform yielding have been also considered (specimen type III). For this type of device, the varying depth $h = h(x)$ of the elementary beams is obtained as a function of the abscissa x with origin at the beam midspan based on a linear variation of the yielding moment $M_y(x)$ as follows:

$$M_y(x) = f_y t\frac{h(x)^2}{6} = Vx = 2\overline{M_y}\frac{x}{L} \tag{1}$$

where f_y is the yield strength of steel, t is the thickness of the elementary beam, V is the shear force, $\overline{M_y} = M_y\left(\frac{L}{2}\right)$ is the yield moment of the end sections, and L is the length of the elementary beam. This leads to:

$$h(x) = \sqrt{12\frac{\overline{M_y}x}{f_y tL}} \tag{2}$$

The cusp at the theoretical zero-depth at midspan is smoothed to a

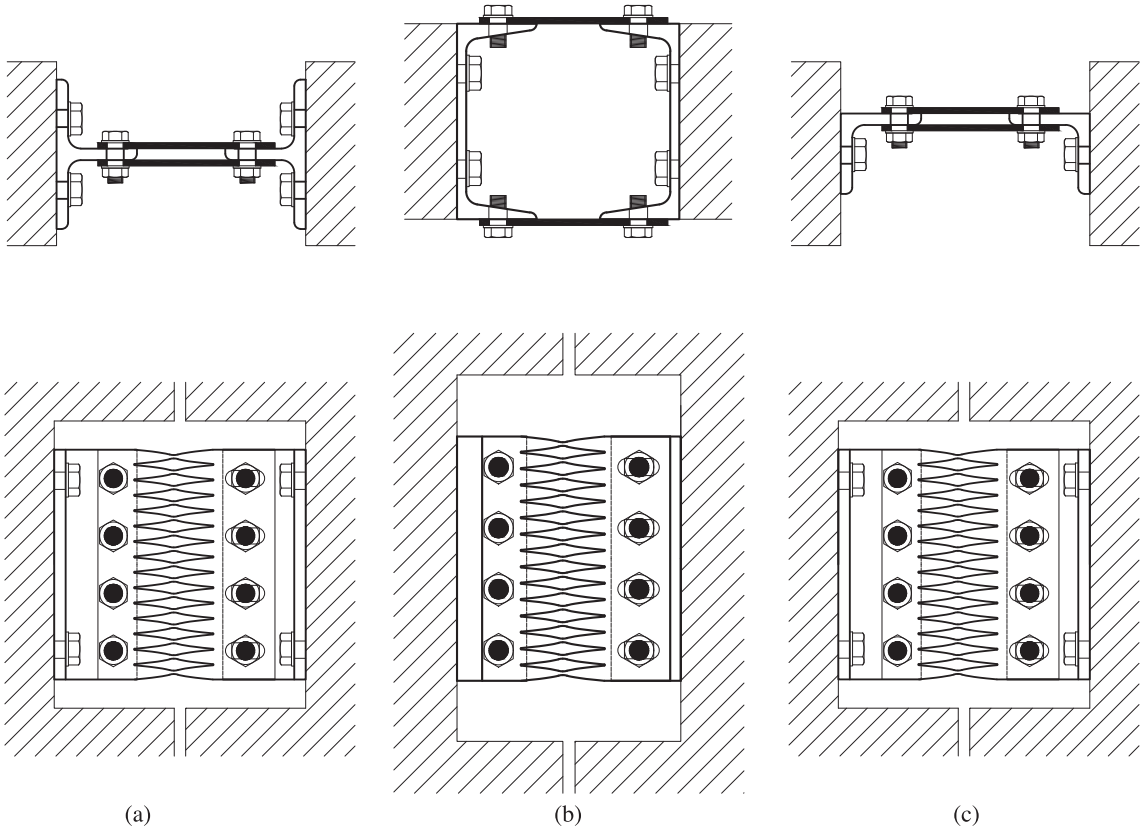

Fig. 2. Assemblage of the MSD with (a) T-shaped, (b) UPN, and (c) angle support steel profiles.

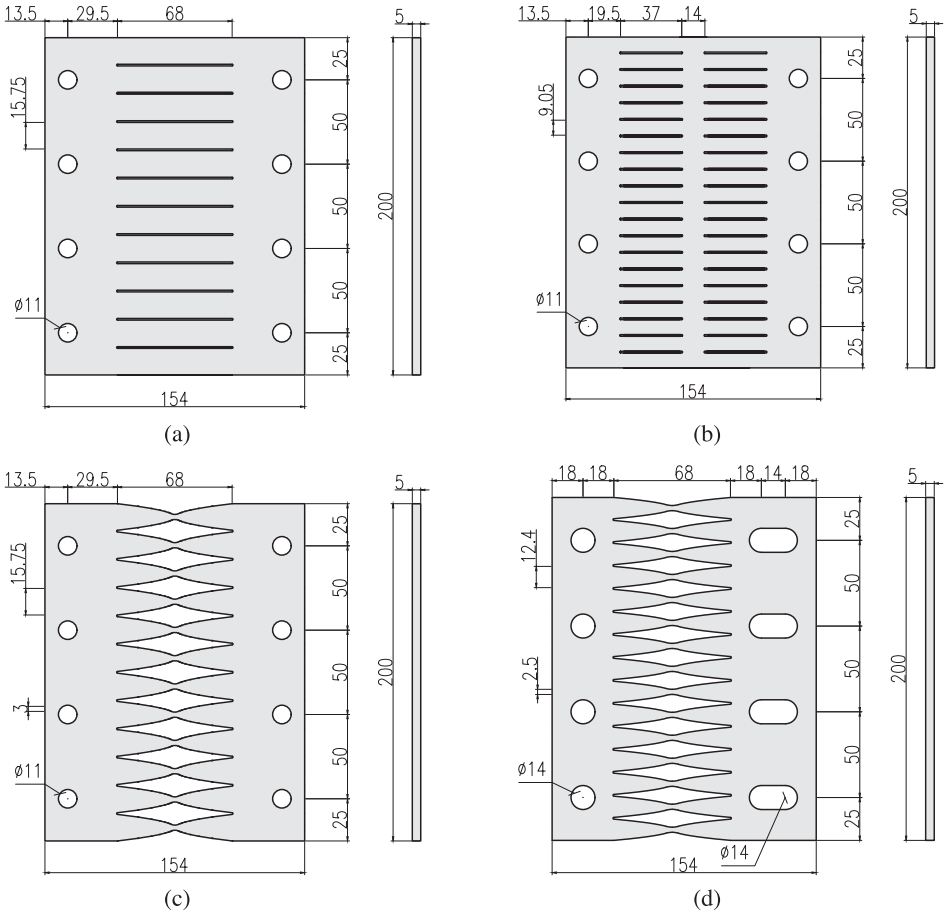

Fig. 3. Geometry and dimensions of the tested MSDs [mm]: (a) one line of beams (I); (b) two lines of beams (II); (c) hourglass-shaped beams (III); (d) hourglass-shaped beams and horizontal slots (IV).

minimum depth equal to 20% of the depth at beam ends to resist the shear stresses.

With respect to the beams with constant depth, the displacement ductility of beams with hourglass profile is larger. Hourglass beam profile plates provided with horizontal slots (specimen type IV) have also been developed to ensure an easier installation with horizontal tolerance. In this case the plate is not symmetric, and the two device plates may be placed in mirrored or inverted configuration, to which corresponds a different horizontal force distribution in the support profiles. All the plates have been designed in order to achieve a similar strength. Specimens type I, II, and III are made of steel grade S235 (nominal characteristic yield strength f_{yk} = 235 MPa). Specimen type IV is made of steel grade S355 (f_{yk} = 355 MPa).

The steel support profiles used in the experimental campaign are shown in Fig. 4. The specimens type I, II, and III are tested in assemblage with T-shaped steel profiles. The web of the profiles is provided with holes for the bolted connection with two plates, placed on the external sides. The specimens type IV are tested in assemblage with UPN steel profiles.

The flanges of the UPN profiles are provided with threaded holes for the direct application of the screws from the external side, with one plate only for each side. In the specimen modified to add dissipation of energy by friction, vertical slots of 20 mm have been milled on the UPN profiles and the plates have been bolted with belleville (cup) and brass washers. Both T-shaped and UPN profiles are provided with holes on the back for the bolted connection with the concrete panel, in which

Fig. 4. Support steel profiles: (a) T-shaped; (b) UPN; (c) UPN with vertical slots.

Table 1
Local tests on MSDs.

MSD type	Test type	Test protocol[a]	Bolt type	Support profiles	Test speed
(I) One line of beams	Cyclic	± 0.5:0.5…10 mm × 3	M10 8.8	T-shaped	2.00 mm/s
	Cyclic	± 0.5:0.5…10 mm × 3	M10 12.9	T-shaped	2.00 mm/s
	Cyclic	± 20 mm × 10	M10 12.9	T-shaped	2.00 mm/s
	Monotonic	–	M10 12.9	T-shaped	0.25 mm/s
(II) Two lines of beams	Cyclic	± 0.5:0.5…10 mm × 3	M10 8.8	T-shaped	2.00 mm/s
	Cyclic	± 0.5:0.5…10 mm × 3	M10 12.9	T-shaped	2.00 mm/s
	Cyclic	± 20 mm × 10	M10 12.9	T-shaped	2.00 mm/s
	Monotonic	–	M10 12.9	T-shaped	0.25 mm/s
(III) Hourglass-shaped beams	Cyclic	± 0.5:0.5…10 mm × 3	M10 8.8	T-shaped	2.00 mm/s
	Cyclic	± 0.5:0.5…10 mm × 3	M10 12.9	T-shaped	2.00 mm/s
	Cyclic	± 0.5:0.5…10 mm × 3	M10 12.9	T-shaped	2.00 mm/s
	Monotonic	–	M10 12.9	T-shaped	0.25 mm/s
(IV) Hourglass-shaped beams with slots	Cyclic	± 0.5:0.5…10 mm × 3	M14 10.9	UPN	2.00 mm/s
	Cyclic	± 20 mm × 10	M14 10.9	UPN	2.00 mm/s
	Monotonic	–	M14 10.9	UPN	0.25 mm/s
	Cyclic	± 0.5:0.5…10 mm × 3	M14 10.9	UPN with slots and brass washers	2.00 mm/s

[a] The first number indicates the first displacement amplitude, the number following the colon indicates the displacement increase, the number following the multiplier indicates the number of cycles per displacement amplitude.

threaded sockets are embedded. All support profiles are made of steel grade S235.

2.2. Test setup

The complete list of experimental tests performed on MSDs is reported in Table 1, including monotonic tests and cyclic tests for imposed displacements at both low and large amplitude. The tests have been carried out on a mono-axial ± 1000 kN Schenck test machine at the Laboratorio Prove e Materiali of Politecnico di Milano and subjected to imposed displacement histories. The connections are tightened through bolts to a strong support made by two L-shaped HEA steel profiles welded together. The L-shaped profiles are then tightened to the machine through nailed thick steel plates provided with large diameter bolts. Fig. 5 shows a picture of the test setup with a device under testing. Two long LVDTs have been installed to measure the relative displacement of the L-shaped steel profiles. The displacement imposed to the device is depured from the small movements occurring at the bolted connection due to the standard hole clearance, as measured by two short LVDTs installed in between each L-shaped steel profile and the device.

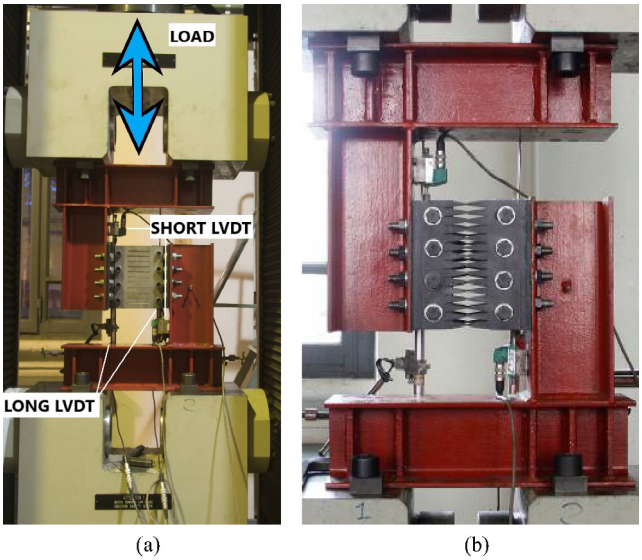

(a) (b)

Fig. 5. Experimental setup for tests on MSDs: (a) overall view, (b) detail of one device and the frame support.

2.3. Monotonic tests

Monotonic tests have been carried out on the four different typologies of MSDs shown in Fig. 3. Fig. 6 shows the specimens in the undeformed configuration and under test at maximum imposed drift. The specimens with constant depth beams (type I and II) are subject to large plastic deformation at the ends and an almost rigid rotation of the central portion. On the contrary, large diffused plasticity is observed within the hourglass-shaped specimens (type III and IV), leading to a better exploitation of the device.

The load versus displacement capacity curves shown in Fig. 7 show a similar tendency. A maximum load of the devices of around 120 kN has been attained for all specimens apart from specimen type III, which attained 103 kN due to the localization of deformation in the central portion of the elementary beam. However, failure of the latter specimen has not been attained. The response is initially significantly stiff, with stiffness depending on the profile for very low displacement, ranging from 23 kN/mm for both devices type I and II, to 28 kN/mm and 20 kN/mm for devices type III and IV, respectively. After an initial elastic branch at small displacements, all capacity curves show a transition to a softer linear branch with an average stiffness of about 12 kN/mm and a subsequent phase of spreading of plasticization with a smooth stiffness softening up to a final branch with an average stiffness of about 1.4 kN/mm. The transition to the final branch started for all specimens at around 5–6 mm of displacement, which corresponds to 7.4–8.8% of drift ratio with respect to the length of the elementary beam (doubled for the specimen type II). All specimens show a large residual plastic deformation after the test, as shown in Fig. 8. The specimens with constant depth beams exhibit a plastic deformation of the plate around the corner holes induced by the inclined force resulting from the combination of the vertical reaction due to shear and the inclined reaction due to rotational equilibrium, as clearly identified by the hole deformation.

2.4. Cyclic tests at low amplitude displacements

Cyclic tests at low amplitude displacements have been carried out to investigate the behavior and stability of the device under serviceability horizontal loads acting on the precast building (e.g. wind loads). Increasing amplitude cycles have been applied, with increments of 0.5 mm up to an amplitude of 10 mm for the devices with constant

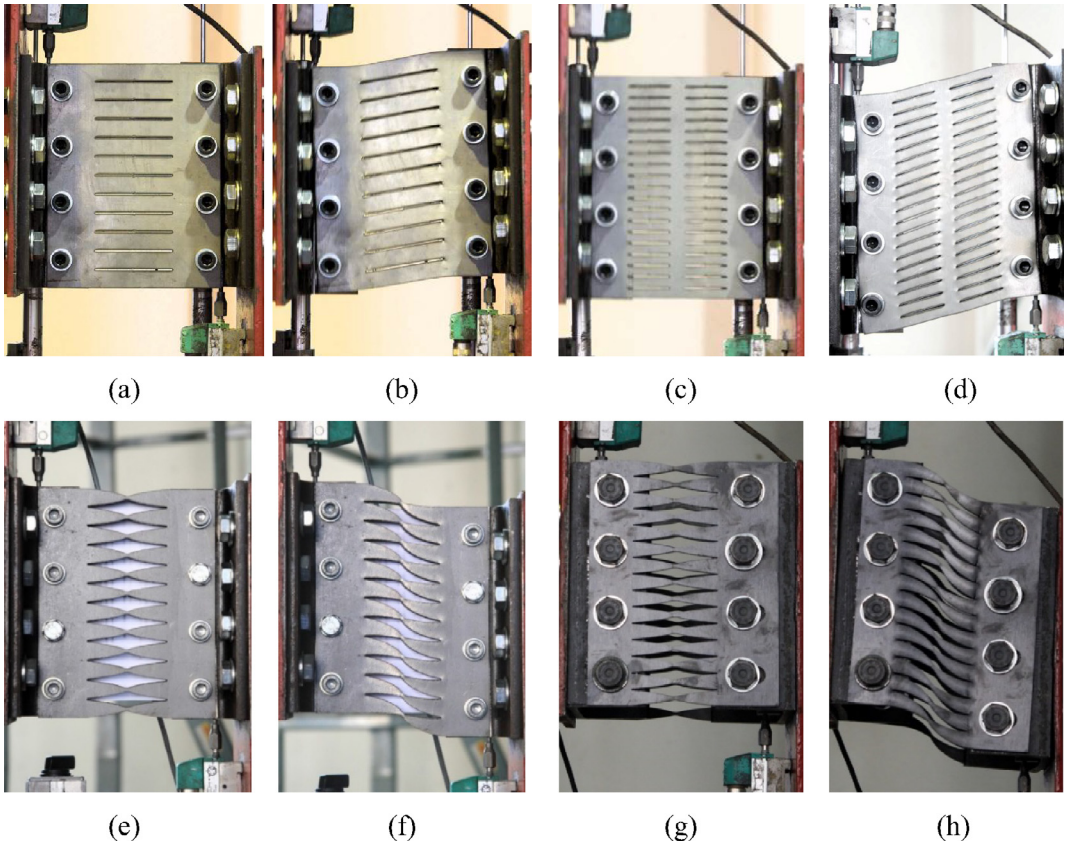

Fig. 6. MSDs in the undeformed configuration and under test at maximum drift: (a, b) one line of beams (I); (c, d) two lines of beams (II); (e, f) hourglass-shaped beams (III); (g, h) hourglass-shaped beams and horizontal slots (IV).

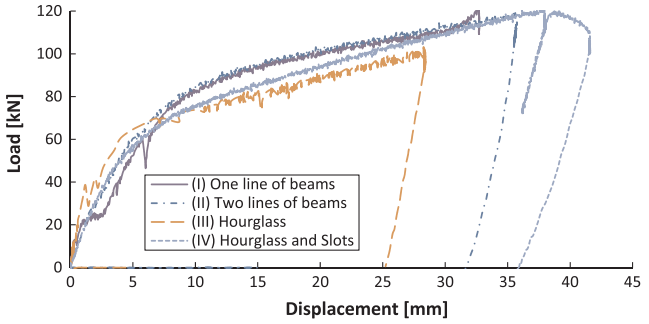

Fig. 7. Load vs displacement diagrams from monotonic tests on MSDs.

depth beams, and increments of 1.0 mm up to failure for the devices with hourglass shaped beams. Each amplitude step was cycled three times. The test speed was kept constant at 2.0 mm/s.

The results are shown in Fig. 9 in terms of load versus displacement diagrams. An initial elastic stiffness of about 27 kN/mm is up to 1.2 mm of displacement for the MSD type I with one line of beams (Fig. 9a). After yielding, plasticization is observed with a smooth stiffness softening starting at around 6 mm of drift. For the MSD type II with two lines of beams (Fig. 9b) the initial elastic stiffness is about 32 kN/mm up to 0.8 mm of drift. The post-yielding branch shows a smooth stiffness softening starting at about 5 mm of displacement. A pinching effect, that is affecting the energy dissipation capacity, is observed for both specimens with constant depth beams. This is likely to be associated with the occurrence of small rigid rotations of the plates due to standard bolt-hole tolerance of one millimeter enlarged by plastic local deformation near the corner holes. The initial elastic stiffness for the MSD type III with hourglass-shaped beams (Fig. 9c) is about 28 kN/mm up to 1.0 mm of drift. After yielding, plasticization is observed with a smooth stiffness softening starting at about 5 mm of displacement. Early failure has been attained with fracture of the central portion of the beams, at about 2 mm from midspan, that started at the last semi-cycle with displacement amplitude of 10 mm, when the specimen entered the phase of complete plasticization. The test on the MSD type IV with hourglass-shaped beams and horizontal slots (Fig. 9d) shows a lower initial elastic stiffness of about 25 kN/mm up to 1.2 mm of drift. The post-yielding branch shows a smooth stiffness softening starting at around 6 mm of drift. Early failure has been obtained with fracture of the beam end cross sections started at 16 mm displacement cycles. Pinching is less pronounced on devices with hourglass-shaped beams, providing a larger energy dissipation capacity, as shown in Fig. 10 by the cumulative dissipated energy curves. The linear trend of these curves prior to onset of failure indicates a stable hysteresis.

It is worth noting that all specimens show cyclic stability for a relatively small range of displacement amplitude (within approximately 10% of drift).

2.5. Cyclic tests at large amplitude displacements

Cyclic tests with ± 20 mm displacement amplitude (corresponding to about 30% of drift for all specimens) cycled ten times have also been carried out in order to investigate the oligo-cyclic stability of the specimens within the phase of complete plasticization. The results are shown in Fig. 11. For device type I (Fig. 11a), the monotonic behavior confirms what previously observed. An early oligo-cyclic failure occurs at the third cycle, with flexural failure at the end sections of all beams. The results of the cyclic tests confirm the previously observed monotonic behavior also for device type II (Fig. 11b). A progressive loss of resistance is observed starting from the fourth cycle, with flexural failure at the end sections of all beams. A relevant pinching effect is also confirmed for both the devices type I and II. The specific energy,

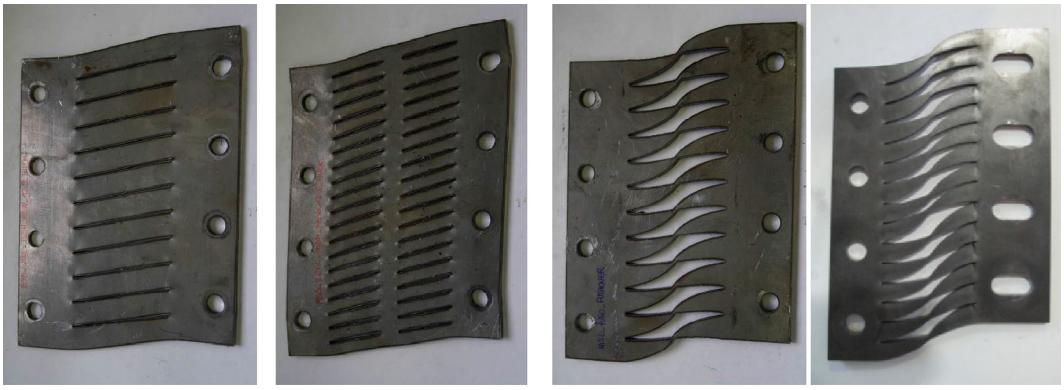

Fig. 8. MSDs with residual plastic deformation after monotonic test: (a) one line of beams (I); (b) two lines of beams (II); (c) hourglass-shaped beams (III); (d) hourglass-shaped beams and horizontal slots (IV).

calculated as the ratio of the area of the first complete cycle (after the initial loading branch) to the area of the rectangle associated with equivalent rigid-plastic behavior, is equal to 0.48 and 0.34 for the device type I and II, respectively. The pinching effect is greatly reduced for the device type IV (Fig. 11c). Pinching does not occur at the first cycles, but an oligo-cyclic failure develops starting at the third cycle. Flexural failure at the end sections of each beam occurs also for device type IV, but plastic strains and hysteresis involve a larger volume of material, with relevant plastic residual deformations distributed over the elementary beams. The specific energy for the device IV is equal to 0.54.

For all tested specimens, the results indicate oligo-cyclic fatigue at large imposed displacements (30% of drift in this specific case) due to failure or strong strength loss attained after only few cycles. Fig. 12 shows the failure modes of the tested devices. For the specimens with constant depth beams (type I and II) the ductility demand concentrates at the beam ends (Fig. 12a, b). For the specimens with hourglass-shaped beams (type III and IV), cross-sectional failure is expected uniformly over the whole beams. However, for the device type III the failure occurs at the beam midspan (Fig. 12c) due to the combination of shear and second order axial stress, to which the central portion is particularly sensitive. Conversely, for the device type IV the failure occurs at beam ends (Fig. 12d) due a slightly larger beam depth adopted at

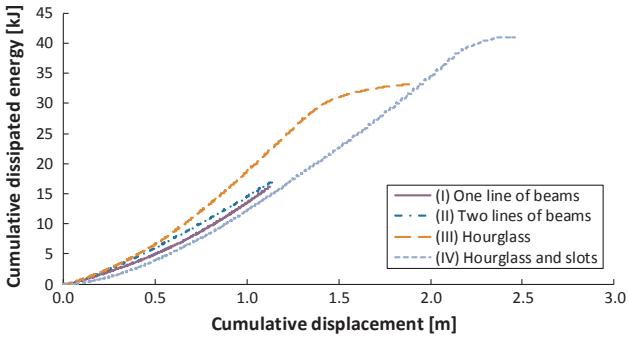

Fig. 10. Cumulative energy dissipation from cyclic tests on MSDs at low amplitude cycles (Fig. 9).

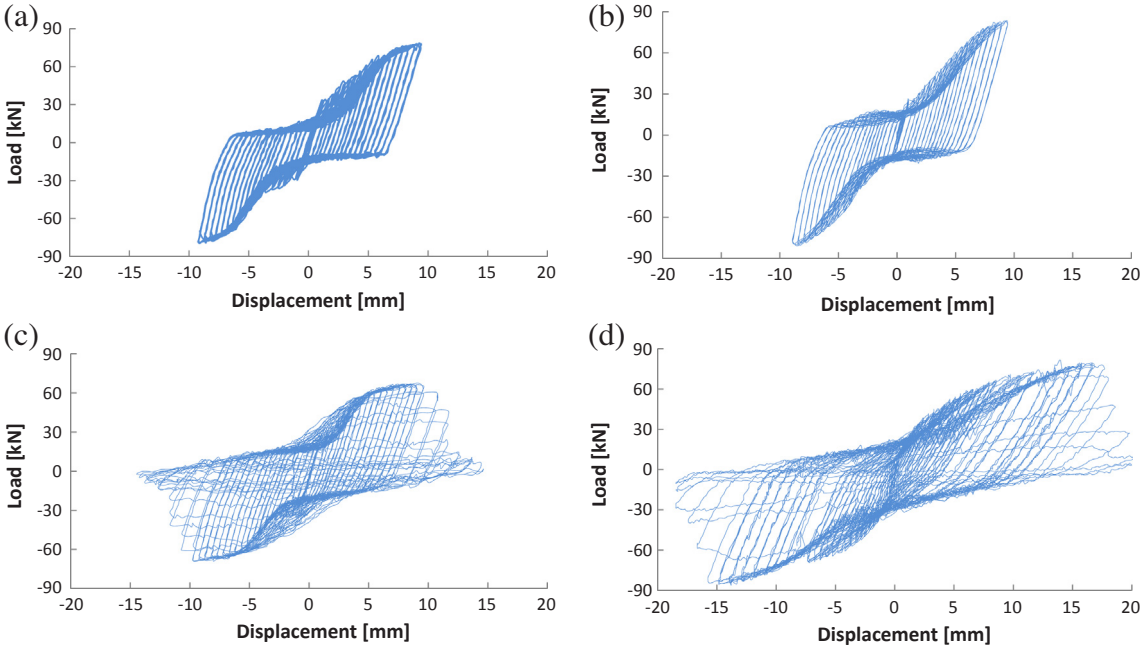

Fig. 9. Load vs displacement diagrams from cyclic tests on MSDs at low amplitude cycles: (a) one line of beams (I); (b) two lines of beams (II); (c) hourglass-shaped beams (III); (d) hourglass-shaped beams and horizontal slots (IV).

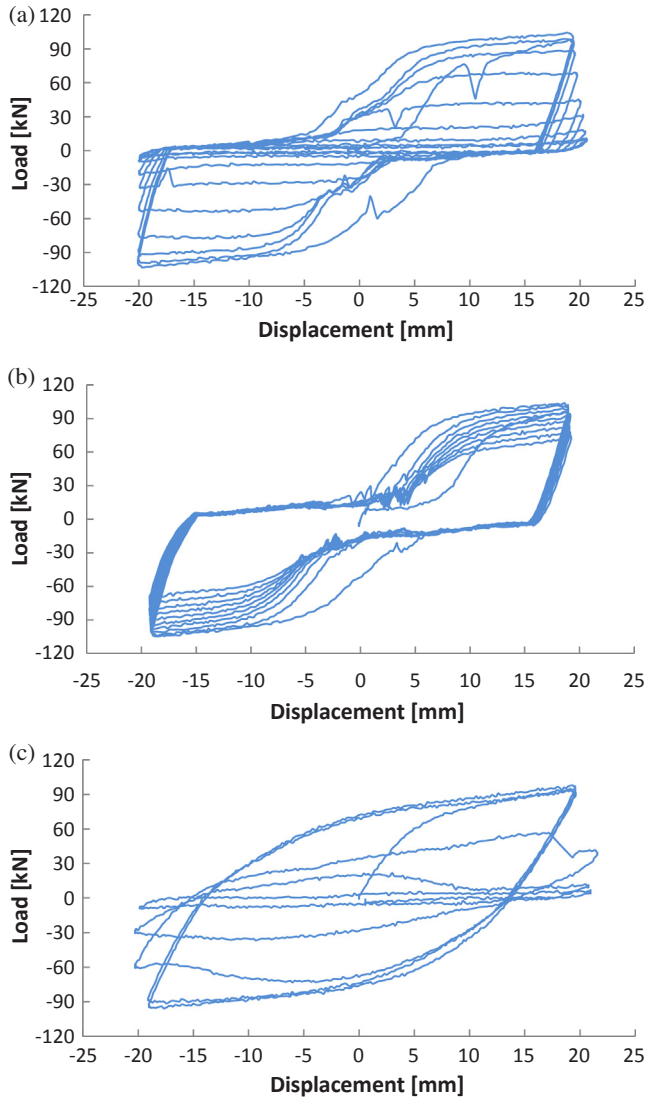

Fig. 11. Load vs displacement diagrams from cyclic tests on MSDs at large amplitude cycles: (a) one line of beams (I); (b) two lines of beams (II); (c) hourglass-shaped beams and horizontal slots (IV).

midspan (beam midspan to end depth ratios of 5.2 for type III and 5.0 for type IV). Failure at beam ends allows for larger displacement capacity and should be addressed in the design of the device.

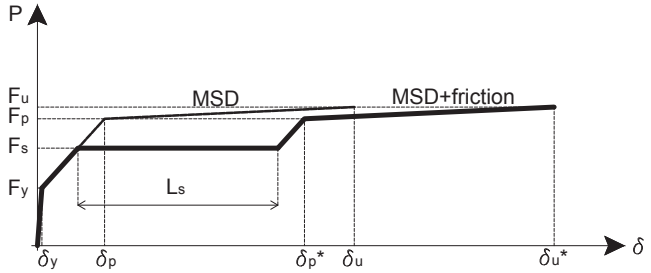

Fig. 13. Comparison of the typical monotonic behavior of MSDs without and with friction energy dissipation capacity.

2.6. MSD with friction energy dissipation capacity

MSDs with friction behavior can be designed to achieve a smooth and flexible elastic branch, due to the functioning of the multiple slit plate, and to increase the displacement capacity by means of a slip load threshold higher than the MSD yield load. The slip load threshold should be included within the phase of spreading of plasticization, in order to avoid oligo-cyclic failure, which typically occurs after entering the phase of complete plasticization. When the slip load threshold is exceeded, the device dissipates energy by friction. The maximum slip is determined by the length of the vertical slots. When it is reached, the plastic mechanism of the multiple slit plate reactivates, allowing for a controlled failure. The monotonic behavior of MSDs without and with friction is compared in Fig. 13, where F_y is the yield load, F_s is the slip load threshold, F_p is the limit load of the phase of development of plasticization, F_u is the ultimate load, δ_y is the yield displacement, and L_s is the maximum slip length, which is equal to the length of the single slot, leading to an increment of the plasticization development phase displacement from δ_p to δ_{p^*} and of the ultimate displacement from δ_u to δ_{u^*}.

A single test based on a cyclic protocol with increasing displacement amplitudes 2.5–5.0–10.0–20.0–40.0 mm has been carried out on a specimen mounted on UPN support profiles provided with net 20 mm long vertical slots (see Fig. 4c) on which two hourglass MSDs with horizontal slots (see Fig. 3d) have been screwed with internal hollowed square brass sheets, in order to achieve cyclic stability under friction, and external belleville washers, in order to minimize the bolt axial losses [16]. Each amplitude is cycled three times. The test speed is kept constant at 2 mm/s. Each of the 8 M14 8.8 bolts per side have been tightened at 100 Nm, in order to obtain a mean slip threshold equal to about 50 kN as proposed by Dal Lago et al. [16]. The results are shown in Fig. 14. The combination of friction and plastic mechanisms brought to large energy dissipation and increased ultimate displacement, with an initial smooth branch depending only on the MSD properties and a final controlled failure with displacement capacity increased by the

Fig. 12. MSDs at failure: (a) one line of beams (I); (b) two lines of beams (II); (c) hourglass-shaped beams (III); (d) hourglass-shaped beams and horizontal slots (IV).

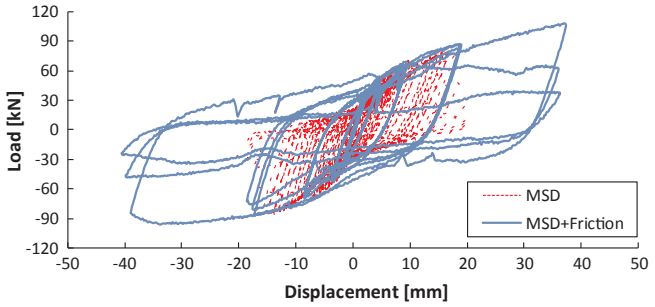

Fig. 14. Load vs displacement diagrams from the cyclic test on the MSD with friction compared with the test results on the same MSD without friction shown in Fig. 9d.

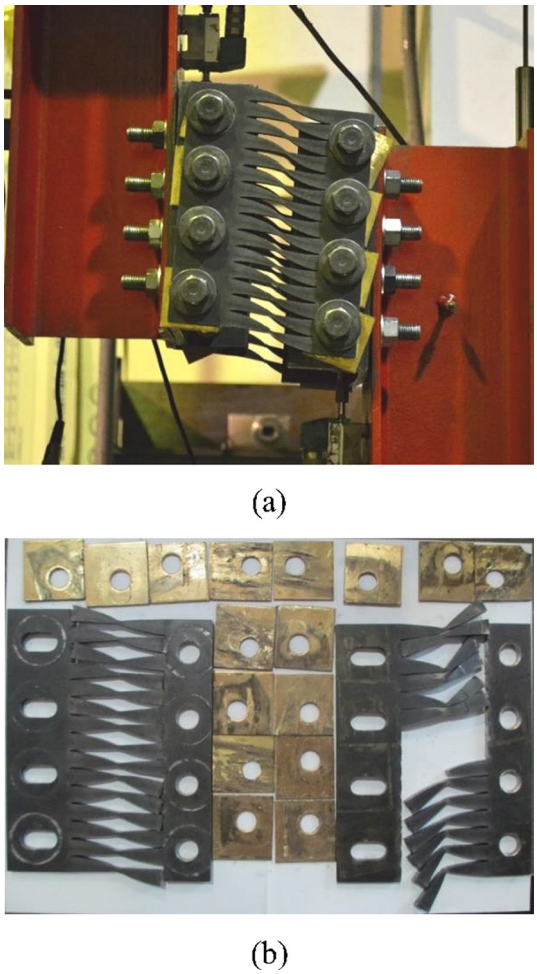

Fig. 15. MSD with friction: (a) deformed shape under testing at +60% of drift; (b) components after testing.

friction slide with respect to the standard MSD. The connection has been able to perform three complete cycles at 30% of drift and one complete cycle at 60% of drift before failure. Fig. 15 shows the connection subjected to large deformation (Fig. 15a) and the components after the test (Fig. 15b). It can be observed that failure occurred at the end sections of the beams. Moreover, the hollowed square brass sheets show that strong abrasion occurred.

3. Structural sub-assembly tests

Two structural sub-assembly cyclic tests have been performed to investigate the mechanical behavior of a MSD when installed in between concrete panels.

3.1. Test setup

The panel sub-assembly test setup is shown in Fig. 16. It is made of two single layer (solid) concrete panels 1290 × 3230 × 160 mm, with an aspect ratio of 2.5. The panels are provided with an upper passing vertical slot in the middle of the panel width, providing a vertical lever arm from the bottom panel-to-foundation connection to the top panel-to-beam connection of about 2700 mm. Three recesses are placed at 1/4, 2/4 and 3/4 of the vertical lever arm at each side of the panels to connect the dissipative devices. The top panel connection is made with round holes hosting steel pins that link the panels to the steel articulated frame through which the imposed displacements are transmitted to the panels. The frame is made with two HEA columns hinged both at the bottom with a strong steel beam and at the top with a double UPN beam surrounding the panels. The hinges are made by steel pins and forks. The frame is connected to a 750 kN horizontal jack fixed to the strong steel braced reaction frame of the lab at a height of 2850 mm, in axis with the beam-to-column pins. A lateral displacement retaining system has been installed in correspondence of the steel beam and attached to it with steel spheres that are fixed to lateral stiff retaining frames. Two vertical long slots are cut in the UPN profiles in order to locate the panel-to-beam connection pins. The panel-to-foundation connection is also hinged with pin and forks. Fig. 17 shows a picture of the assembled setup.

The three recesses at the panel side are used to host different types of dissipative connectors [27,28]. In the experimental tests presented in this paper, a single MSD with hourglass-shaped elementary beams and horizontal slots (type IV, Fig. 3d), mounted in inverted configuration on UPN support profiles provided with threaded holes, has been bolted in the bottom panel recess. Fig. 18a shows a picture of the assembled connection.

3.2. Experimental results

A cyclic experimental test has been carried out with increasing horizontal displacement amplitudes 5.25–10.5–21–42–84 mm, with three cycle repetitions. The set of amplitudes has been defined based on the cyclic protocol adopted for other dissipative connections [16] to allow for a direct comparison of the results [27,28]. A further test performing a single cycle with new plates at ± 61 mm horizontal drift has been also performed.

The results are shown in Fig. 19 in terms of load versus vertical relative displacement (Fig. 19a), related to the device deformation, and load versus horizontal top displacement (Fig. 19b), related to the global frame. These results are in accordance with the local behavior of the connection characterized through local tests, with an initial stiffness of the device of about 10 kN/mm, a well-defined and stable backbone curve, and good energy dissipation capacity. Fig. 18b shows a deformed configuration at large displacement amplitude. Early oligo-cyclic failure in correspondence of the beam ends has been attained at the first reloading semi-cycle with maximum displacement amplitude, after entering the phase of complete plasticization (Fig. 19).

Compared to the local behavior (Fig. 19a), the global behavior is influenced by the elastic stiffness of the whole structural sub-assembly (Fig. 19b), which shall be taken into account for a proper estimation of elastic stiffness and energy dissipation properties.

4. Design rules

The design ultimate strength of a MSD can be calculated based on the geometry of the plates and the steel strength. The ultimate shear strength V_u of a single elementary beam can be obtained according to the equilibrium of the beam under imposed vertical displacement as follows:

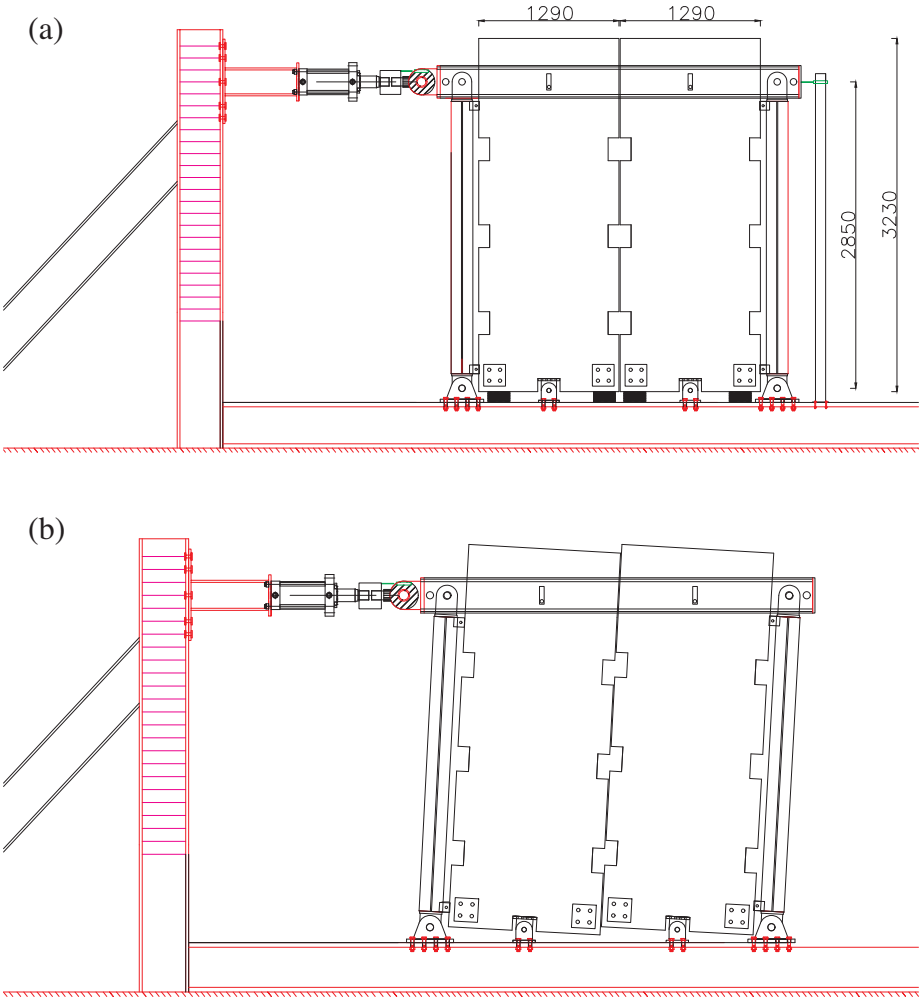

Fig. 16. Experimental setup for the two-panel sub-assembly tests [mm]: (a) undeformed and (b) deformed configurations.

Fig. 17. View of experimental setup for the two-panel sub-assembly tests.

$$V_u = 2\frac{\overline{M_y}}{L}\phi_{pl}\phi_{os}\psi \tag{3}$$

where $\overline{M_y}$ is the yield moment of the end cross-section, L is the length of the elementary beam, ϕ_{pl} is the plasticity factor (equal to 1.5 for rectangular sections), ϕ_{os} is the over-strength factor given by the ratio between ultimate and yield strength of steel (equal to 1.53 for S235 and 1.44 for S355 [30]), and ψ is a non-contemporaneity factor which can be considered equal to 0.94 for standard steel grades [24]. This formulation is valid for both constant-depth and hourglass-shaped beam profiles.

The ultimate shear strength $V_{u,tot}$ of the connection can hence be calculated as follows:

$$V_{u,tot} = n_p n_b V_u \tag{4}$$

where n_p is the number of plates ($n_p = 2$ in the proposed connection arrangement), and n_b is the number of elementary beams in the direction of the imposed displacement.

Table 2 shows the results of the predictions based on the design rules described above compared with the experimental results obtained from cyclic tests at low displacement amplitude. The slight underestimation provided by the design rule for the devices type I, II, and IV can be related to a steel strength larger than the nominal characteristic values. The design procedure slightly overestimates the results of the test on specimen type III, which can be due to the failure of the beams at midspan mainly subjected to shear stress. To avoid this type of failure, the following minimum beam depth d_{min} at midspan should be adopted:

$$d_{min} = \frac{\sqrt{3}V_u}{f_y t} \tag{5}$$

where t is the thickness of the plate, and f_y is the yield strength of steel.

It is worth noting that pushover and oligo-cyclic tests at large amplitude displacements show significantly greater strength values (up to 50%), mainly due to geometrical second order effects. An overstrength factor of 1.50 is suggested in the capacity design of the other connections, for instance the bolts that connect the plates to the support profiles.

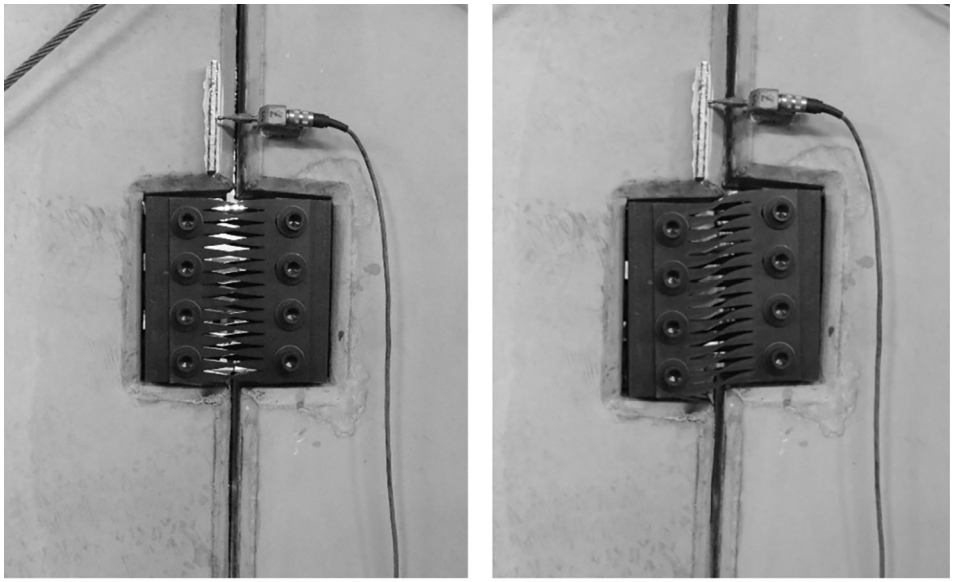

Fig. 18. Detail of the MSD with hourglass-shaped beams and horizontal slots (IV) installed in between the panels on the structural sub-assembly: (a) undeformed and (b) deformed configurations.

5. Conclusions

Steel Multiple Slit Devices (MSDs) are proposed to be used as dissipative shear connectors bolted in between precast concrete panels to improve the seismic performance of precast structures. An experimental campaign has been carried out at Politecnico di Milano to characterize the mechanical behavior of MSDs with different slit patterns and related profiles of the elementary beams, including constant depth and hourglass-shaped beam profiles leading to optimized distribution of plastic strain along the length of the beam. A specimen combining energy dissipation through plasticity and friction with enhanced displacement capacity has been also proposed and tested. Both monotonic and cyclic local tests on single devices and cyclic full-scale structural panel sub-assembly tests have been performed.

The results of local monotonic tests show that all profiles are characterized by a stiff elastic phase, followed by a pseudo-linear phase of development of plasticization, to which corresponds a relevant increase of strength due to the combination of plastic stress distribution and material over-resistance. A final softer pseudo-linear branch after full plasticization is observed up to failure, which has been attained for most connections at a drift larger than 40% with reference to the single elementary beam span, providing a remarkable ductility. For the plates with constant-depth beam profile, local deformation of the contact surface with the connecting bolts has been observed at the end of the tests.

Table 2
MSD shear strength: comparison of experimental results from cyclic tests at small displacement amplitude with analytical predictions from the design rules.

	(I) One line of beams	(II) Two lines of beams	(III) Hourglass-shaped beams	(IV) Hourglass-shaped beams with slots
Exp. [kN]	80	84	69	86
Num. [kN]	73	74	73	80
Exp./num.	1.10	1.14	0.95	1.08

The results from cyclic tests with low-displacement protocol show that all profiles have a stable plastic hysteretic behavior and a negligible strength/stiffness degradation up to about 10% of drift. The plastic local deformation around the external bolts for constant depth beam profiles introduced a pinched tendency in the hysteresis, whilst it is not observed in the devices with hourglass-shaped beams. Therefore, the latter provided a larger dissipation of energy.

The results from the cyclic tests with large-displacement protocol confirmed that the hysteresis at drift larger than 10%, entering the phase of complete plasticization, may become unstable, and early failure or severe strength loss of the specimens has been attained after few cycles of hysteresis performed at 30% of drift.

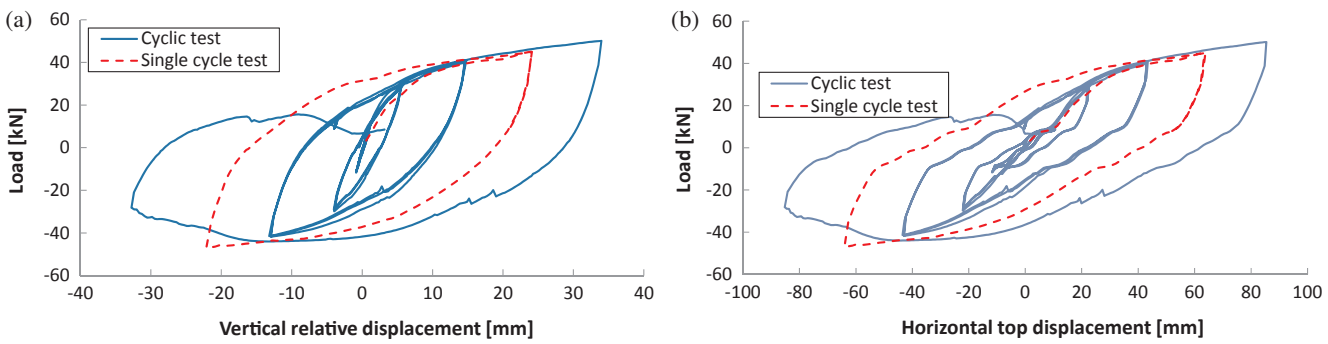

Fig. 19. Cyclic test on the two-panel structural sub-assembly: (a) load vs vertical relative displacement diagrams; (b) load vs horizontal top displacement.

The cyclic test on the specimen with combined friction and plastic dissipation showed how the introduction of few technological modifications, if properly calibrated, can increase the displacement capacity of the device without jeopardizing its energy dissipation properties.

The results from cyclic tests on full-scale structural sub-assembly of concrete panels with a MSD with hourglass-shaped beams provided a confirmation of the large energy dissipation properties of the studied device and a satisfactory behavior of the components used to connect the device to the concrete panels. The global hysteretic shape is affected by the elastic deformability of the overall structural system, including the sub-assembly members and their connections.

More efficient shapes and topologies of the multiple slit plates have been identified by means of evolutionary structural optimization methods and are currently under investigation [31]. Further numerical and experimental research is needed along these lines.

Acknowledgements

The work presented in this paper has been funded mainly by the European Commission within the FP7-SME-2011 SAFECLADDING research project (Grant agreement No. 314122, 2012), and partially by the Italian Department of Civil Protection (DPC) and the Italian Laboratories University Network of Earthquake Engineering (ReLUIS) within the research program DPC-ReLUIS 2014-2016. The financial supports of the funding institutions are gratefully acknowledged. Gratitude and appreciation are expressed to Marco Lamperti Tornaghi, Silvia Bianchi, Giulia Marelli, Giulia Mariani Orlandi, and Alessandro Rocci for their contributions to the execution of the tests. BS Italia and Styl-Comp companies are also gratefully acknowledged for the careful production of specimens and setup members, with special thanks to Claudio Pagani and Enzo Ruggeri.

References

[1] Whittaker AS, Bertero VV, Thompson CL, Alonso LJ. Seismic testing of steel-plate energy dissipating devices. Earthq Spectra 1991;7(4):563–604.
[2] Xia C, Hanson RD. Influence of adas element parameters on building seismic response. ASCE J Struct Eng 1992;118(7):1903–18.
[3] Aiken ID, Nims DK, Whittaker AS, Kelly JM. Testing of passive energy dissipation systems. Earthq Spectra 1993;9(3):335–70.
[4] Tsai K, Chen H, Hong C, Su Y. Design of steel triangular plate energy absorbers for seismic-resistant construction. Earthq Spectra 1993;9(3):505–28.
[5] Soong TT, Spencer Jr BF. Supplemental energy dissipation: state-of-the-art and state-of-the-practice. Eng Struct 2002;24(3):243–9.
[6] Kim YJ, Ahn TS, Bae JH, Oh SH. Experimental study of using cantilever type steel plates for passive energy dissipation. Int J Steel Struct 2016;16(3):959–74.
[7] Chan RWK, Albermani F. Experimental study of steel slit damper for passive energy dissipation. Eng Struct 2008;30(4):1058–66.
[8] Chan RWK, Albermani F, Williams MS. Evaluation of yielding shear panel device for passive energy dissipation. J Constr Steel Res 2009;65:260–8.
[9] Chan RWK, Albermani F, Kitipornchai S. Experimental study of perforated yielding shear panel device for passive energy dissipation. J Constr Steel Res 2013;91:14–25.
[10] Oh SH, Kim YJ, Ryu HS. Seismic performance of steel structures with slit dampers. Eng Struct 2009;31:1997–2008.
[11] Ghabraie K, Chan R, Huang X, Xie YM. Shape optimization of metallic yielding devices for passive mitigation of seismic energy. Eng Struct 2010;32(8):2258–67.
[12] Briones BA, de la Llera JC. Analysis, design and testing of an hourglass-shaped copper energy dissipation device. Eng Struct 2014;79:309–21.
[13] Ma X, Borchers E, Pena A, Krawinkler H, Billington S, Deierlein GG. Design and behavior of steel shear plates with openings as energy dissipating fuses. Report 173, Stanford, CA, USA: Department of Civil and Environmental Engineering, Stanford University; 2010. p. 118.
[14] Karavasilis TL, Kerawala S, Hale E. Hysteretic model for steel energy dissipation devices and evaluation of a minimal-damage seismic design approach for steel buildings. J Constr Steel Res 2012;70:358–67.
[15] Lee CH, Kim J, Kim DH, Ryu J, Ju YK. Numerical and experimental analysis of combined behavior of sheartype friction damper and non-uniform strip damper for multi-level seismic protection. Eng Struct 2016;114:75–92.
[16] Dal Lago B, Biondini F, Toniolo G. Friction-based dissipative devices for precast concrete panels. Eng Struct 2017;147:356–71.
[17] Dal Lago B, Biondini F, Toniolo G. Experimental investigation on steel W-shaped folded plate dissipative connectors for precast cladding panels. J Earthq Eng 2017. http://dx.doi.org/10.1080/13632469.2016.1264333.
[18] Martinelli P, Mulas MG. An innovative passive control technique for industrial precast frames. Eng Struct 2010;32:1123–32.
[19] Sorace S, Terenzi G. Existing prefab R/C industrial buildings: seismic assessment and supplemental damping-based retrofit. Soil Dyn Earthq Eng 2017;94:193–203.
[20] Yüksel E, Karadoğan F, Özkaynak H, Khajehdehi A, Güllü A, Smyrou E, et al. Behaviour of steel cushions subjected to combined actions. Bull Earthq Eng 2017;16(2):707–29.
[21] Belleri A, Marini A, Riva P, Nascimbene R. Dissipating and re-centring devices for portal-frame precast structures. Eng Struct 2017;150:736–45.
[22] Magliulo G, Cimmino M, Ercolino M, Manfredi G. Cyclic shear tests on RC precast beam-to-column connections retrofitted with a three-hinged steel device. Bull Earthq Eng 2017;15(9):3797–817.
[23] Biondini F, Dal Lago B, Toniolo G. Role of wall panel connections on the seismic performance of precast structures. Bull Earthq Eng 2013;11(4):1061–108.
[24] Dal Lago B. Seismic performance of precast structures with dissipative cladding panel connections. [Ph.D. thesis], Politecnico di Milano, Department of Civil and Environmental Engineering; 2015. p. 284.
[25] Toniolo G, Dal Lago B. Conceptual design and full-scale experimentation of cladding panel connection systems of precast buildings. Earthq Eng Struct Dyn 2017;46(14):2565–86.
[26] Negro P, Lamperti Tornaghi M. Seismic response of precast structures with vertical cladding panels: the SAFECLADDING experimental campaign. Eng Struct 2017;132:205–28.
[27] Biondini F, Dal Lago B, Toniolo G. Experimental and numerical assessment of dissipative connections for precast structures with cladding panels. In: 2nd European Conference on Earthquake Engineering and Seismology (2ECEES), Istanbul, Turkey, August 25–30, 2014, Paper No. 2168.
[28] Biondini F, Dal Lago B, Toniolo G. Experimental tests on dissipative cladding connection systems of precast structures. In: 16th World Conference of Earthquake Engineering (16WCEE), Santiago (Chile), January 9–13, 2017, Paper No. 933.
[29] Colombo A, Negro P, Toniolo G. The influence of claddings on the seismic response of precast structures: the Safecladding project. In: 2nd European Conference on Earthquake Engineering and Seismology (2ECEES), Istanbul, Turkey, August 25–39, 2014, Paper No. 1877.
[30] EN 1993-1-1:2005. Eurocode 3: Design of steel structures – Part 1–1: general rules and rules for buildings. Brussels, Belgium: European Committee for Standardization; 2005. p. 91.
[31] Bianchi S, Marelli G, Biondini F, Titi A. Optimization of dissipative panel-to-panel connections of precast structures. In: Italian Concrete Days 2016, Rome, Italy, October 26–28, 2016, Paper No. 39 [in Italian].